

Multi-robot workspace design and motion planning for package sorting

Peiyu Zeng^{1*}, Yijiang Huang^{2*}, Simon Huber², Stelian Coros²

Abstract—Robotic systems are routinely used in the logistics industry to enhance operational efficiency, but the design of robot workspaces remains a complex and manual task, which limits the system’s flexibility to changing demands. This paper aims to automate robot workspace design by proposing a computational framework to generate a budget-minimizing layout by selectively placing stationary robots on a floor grid, which includes robotic arms and conveyor belts, and plan their cooperative motions to sort packages from given input and output locations. We propose a hierarchical solving strategy that first optimizes the layout to minimize the hardware budget with a subgraph optimization subject to network flow constraints, followed by task allocation and motion planning based on the generated layout. In addition, we demonstrate how to model conveyor belts as manipulators with multiple end effectors to integrate them into our design and planning framework. We evaluated our framework on a set of simulated scenarios and showed that it can generate optimal layouts and collision-free motion trajectories, adapting to different available robots, cost assignments, and box payloads. A supplementary video demonstrating the proposed framework and its results is available on YouTube at <https://www.youtube.com/watch?v=OvYzXEfv3dk>.

Index Terms—Multi-Robot Layout Design; Task and Motion Planning; Conveyor System; Cooperative manipulation; Robotics and Automation in Logistics

I. INTRODUCTION

Robotic systems are routinely used in the logistics industry to enhance operational efficiency, which often involves the use of conveyor belts and robotic arms to facilitate the sorting and transportation of packages. Regardless of the specific machinery employed, every logistics workflow requires a well-designed workspace that effectively meets operational demands. However, designing such workspaces remains a complex and manual task, which limits the system’s flexibility when adapting to changing demands, for example, a sudden influx of goods to a new destination that requires adding a new output port. To enable adaptive robotic sorting systems that can rapidly reconfigure their layout and function to new demands, this work presents a computational framework to design and plan both the robots’ workspace and motions. We focus on designing the fully actuated components of a workspace, i.e., the selection and placement of stationary robots on a floor grid, which

¹ Peiyu Zeng is with the Department of Mechanical and Process Engineering, ETH, Zurich, Switzerland. pezeng@ethz.ch

² The authors are with the Department of Computer Science, ETH, Zurich, Switzerland. {yijiang.huang; simon.huber; scoros}@inf.ethz.ch

* These authors contributed equally.

This work has been submitted to the IEEE for possible publication. Copyright may be transferred without notice, after which this version may no longer be accessible.

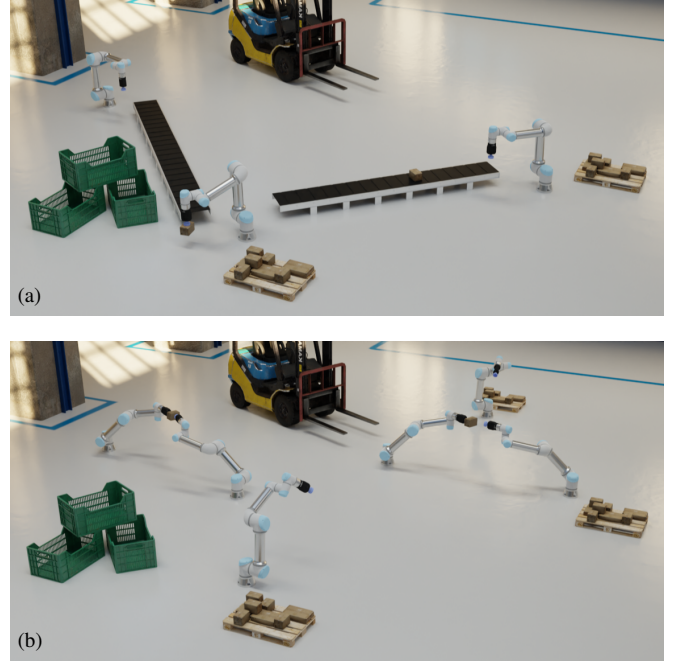


Fig. 1: Multi-robot logistic workspaces generated (a) before and (b) after adding an output location.

include robotic arms and conveyor belts, and assume that the non-actuated components are fixed, such as input ports and output containers. The proposed design framework optimizes a robot layout to minimize hardware budget and computes a collaborative plan of the deployed robots to deliver boxes from a given input location to several output locations.

Designing a multi-stationary robot workspace that minimizes the hardware budget requires solving a challenging optimization problem that involves discrete and continuous variables: one needs to decide which robots to use and where to put them on the floor, while ensuring valid robot motions exist to deliver boxes to targets. Our key insight is to decouple the layout optimization from motion planning, and build a graph to model the flows of goods for each possible robot placement. Then, we formulate the layout design problem as finding a minimum-cost subgraph while ensuring flows to all destinations, which can be solved using Mixed-Integer Linear Programming (MILP). With the computed workspace layout, we generate task allocation and scheduling, then compute robot delivery motion with trajectory optimization.

Our core contributions include:

- We decouple layout optimization and motion planning, and propose a new mathematical formulation for finding cost-minimizing multi-robot layout as a subgraph

optimization subject to graph flow constraints.

- We model conveyor belts as manipulators with multiple end effectors, enabling interconnected conveyor belts to be integrated into the layout design and motion planning alongside other robot arms.
- We provide simulated evaluations of our method responding to different available robots, cost assignments, and box payloads. We show our layout optimization formulation can find optimal layout designs faster and scale better than an A* search.

II. RELATED WORK

Layout optimization for robot manipulators involves placing robots within a workspace to maximize task efficiency and operational robustness. A key metric in this process is reachability, which evaluates a robot's ability to manipulate objects across different positions and orientations within its operational domain. In [1], a directional reachability map is introduced to represent the manipulatable regions, which can be precomputed per robot on a voxelized space [2]. A reachability score can be derived for optimizing the robot placement to ensure multi-directional manipulability [3]. In these previous works, the layout only involves placing one or two robots working in close proximity, and the interaction between robots plays no role in the layout. In contrast, our work considers placing robots on a large open floor where a successful delivery requires multi-agent collaborative manipulation, and the number and types of robots are both unknown in the layout optimization.

Co-design of robots and trajectories considers co-optimizing a robot's design parameters (e.g., link lengths) with its motion trajectories or control policy, so that the robot's hardware can be tailored to the specific deployed environment, enhancing performance and reducing energy consumption. Robot link lengths have been co-optimized with joint trajectories using sensitivity analysis [4] or inverse kinematic methods [5], but typically assuming that the end-effector trajectories are provided. [6] embeds design parameter optimization into a sequential manipulation formulation to optimize the robot arm's morphology for a task ensemble. [7] co-optimizes links and motor configuration of animatronic figures with motion trajectories using a search with a custom-designed heuristic. While previous work focuses on a single robot's "intrinsic" design parameters, such as link lengths, our work focuses on designing the layout of multiple robots, which could be regarded as "extrinsic" properties of an agent in a larger system.

Task and motion planning This work considers multiple robots delivering boxes, a long-horizon manipulation task that requires coordination of multiple agents' tasks and motions. Task And Motion Planning (TAMP) jointly computes high-level action sequences along with feasible motion paths to realize these actions [8]. Classical AI search algorithms for task planning are combined with sampling-based [9] or optimization-based method [10] for motion planning to allow reasoning at both levels simultaneously. Manipulation planning [11] is a specific class of problems that can be addressed

by TAMP methods. While planning for a single manipulator is already challenging, TAMP for multiple agents puts an additional burden on the planning algorithms [12]. In [13], a differentiable TAMP algorithm is proposed to allow handover between manipulators to emerge automatically by treating task assignment as implicit, time-dependent functions to be optimized. For pick and place problems involving multiple robots and handovers, less general yet effective heuristic and sampling strategies have been proposed [14]. In this work, we consider a new problem that couples TAMP and robot workspace design. We solve the problem hierarchically: since we only consider delivering one box at a time, once an optimal layout is obtained, the task scheduling and motion planning can be solved separately.

Multi-agent path finding and layout design Coupling multi-agent path planning and robot workspace design has been investigated in the context of robotic warehouses. [15], [16] propose learning-based methods to optimize the layout to maximize the throughput of 2D mobile robots in a warehouse using a multi-agent path-finding algorithm as the performance evaluator. [17], [18] consider the environment layout as decision variables, jointly optimizing it with agent performance and environment cost through reinforcement learning to achieve high performance in multi-agent path-finding. Although their problem is similar to ours on a conceptual level, they focus on routing paths for mobile robots on a 2D grid. In contrast, our work focuses on finding the minimum-cost layout for robotic manipulators.

III. OVERVIEW

Our goal is to design a multi-robot delivery system that can send N boxes from a single input collection point to multiple destinations on a factory floor. We assume that the robots can only be installed on a discrete grid of points $P \subset \mathbb{R}^2$. We can assign robots from a given set of available robot types \mathcal{R} , without a limit placed on the number of each type. In this work, we consider the delivery of each box separately, i.e., boxes are not flowing in with a specific order, and thus focus on the geometric feasibility of the system to deliver boxes. The decision variables include:

- *Robot layout assignment*: let $a : P \rightarrow \mathcal{R} \cup \{Nil\}$ be the assignment function that associates a grid point p with an appropriate robot type in \mathcal{R} . Nil means no robot is assigned;
- *Task schedules*: for delivering box i , let $s^i : [0, T] \rightarrow \mathcal{R}$ be the scheduling function that maps time t to robots that are actively grasping box i .
- *Trajectory* of each robot: $\mathbf{x}_{r_j} : [0, T] \rightarrow \mathbb{R}^{d_j}$, where d_j is the degree of freedom of robot r_j .

Given the input and output locations of the box, the points of the grid, and the set of available robots, we aim to minimize the total robot budget while ensuring feasible robot

trajectories to deliver each box:

$$\min_{a,s,\mathbf{x},\mathbf{y}} \sum_{p \in P} \text{COST}(a(p)) \quad (1a)$$

$$s.t. \quad \forall i \in 1, \dots, N$$

$$g_i(\mathbf{x}(t)) \leq 0, \forall t \in [0, T] \quad (1b)$$

$$c_i(\mathbf{y}(t), \mathbf{x}_j(t)) = 0, \forall t, j \text{ s.t. } r_j = s^i(t) \quad (1c)$$

$$c_i^*(\mathbf{y}(t)) = 0, \forall t \in \{0, T\} \quad (1d)$$

where \mathbf{y} is the poses of boxes, the Eq. 1b denotes general constraints that ensure the robot trajectory for delivering box i is collision-free and respects joint limits. Equation 1c defines the grasping relationship between the box i and the active robot manipulator r_j . Equation 1d defines the initial and target poses of each box i .

Solving the problem described in Eq. 1 in a fully joint and global manner is intractable since it is a mixed-integer optimization problem with non-convex constraints, and finding globally optimal solutions is challenging. We present our approach to decompose the problem into three subproblems: ① layout optimization, ② task scheduling, and ③ motion planning. This hierarchical solution allows us to first solve the layout optimization to *global optimum* in terms of robot costs on a simplified graph model while ensuring task and motion feasibility (Section IV-A). Then, we use a simple heuristic to schedule the tasks to robots on the computed layout (Section IV-B), followed by multi-agent motion planning using trajectory optimization (Section IV-C).

IV. METHOD

A. Robot Layout Optimization

The layout optimization concerns finding a minimum-budget robot assignment that kinematically delivers each box from the input location to its output location.

Our key insight is to build a graph on a ground set of all potential robot layout assignments and model the layout optimization problem as identifying a minimum-weight, connected subgraph. This graph formulation allows us to reduce the full multi-robot motion planning defined in Eq. 1 that can only be computed *after* an assignment is given into simple pair-wise reachability checks that can be *precomputed*.

Formally, we aim to build a directed graph $G = (V, A)$, where the vertex set $V = V_{io} \cup V_{\mathcal{R}}$ contains input/output locations V_{io} and all possible robot assignment $V_{\mathcal{R}}$. The robot arrangement ground set $V_{\mathcal{R}}$ is constructed by filling each grid point $p \in P$ with all robots in \mathcal{R} , with multiple vertices occupying the same physical grid point.

Each arc $a = (v_i, v_j)$ of the arc set A indicates that a vertex v_i can be reached by v_j while satisfying the kinematic and collision constraints. This is checked using the trajectory optimization technique described in Section IV-C limited to a single time step of handover. The examples of the results of the reachability check are shown in Fig. 2. Fig. 3a shows a visual example of the robot layout ground set, and Fig. 3b shows the corresponding directed graph.

Since all kinematic constraints are embedded in the reachability graph, the layout optimization can be simplified as

extracting a minimum-cost subgraph, while ensuring that there exist paths to connect the input to all outputs. An example feasible subgraph is colored red in Fig. 3b. By assigning the cost of robots as the corresponding vertex weights w_v , our goal becomes minimizing the total vertex weight in a subgraph where all output locations are connected to the input location with paths, which can be formulated as:

$$\min_{G'=(V',A')} \sum_{v \in V'} w_v \quad (2a)$$

$$s.t. \quad V' \subseteq V, A' \subseteq A \quad (2b)$$

$$V_{io} \subset V' \quad (2c)$$

$$\exists \psi = (v_1, v_2, \dots, v_m) \text{ s.t. } (v_i, v_{i+1}) \in A', \\ v_1 = v_i, v_m = v_o, \forall v_i \in V_{in}, \forall v_o \in V_{out} \quad (2d)$$

Equation 2 can be further formulated as a mixed-integer linear programming (MILP) problem using network flow. The key idea is to transform vertex weights into arc weights and introduce binary arc selection variables to control the arcs' flow capacity. We first substitute every robot vertex $v \in V_{\mathcal{R}}$ with two vertices inheriting inbound arcs and outbound arcs, respectively, and an auxiliary arc a connecting them with arc weight inherited from the original vertex: $w_a = w_v$. Then, the original arc set A is augmented with the set of auxiliary arcs A_{aux} .

Let $s_a \in \{0, 1\}$, $a \in A$ be the binary variable indicating whether the arc a is selected in the subgraph. To model Eq. 2d, we introduce N commodity flows, each starting from the input location and ending at one of the output locations. Let $f_{a,i}$, $a \in A$, $i \in \{1, 2, \dots, N\}$ be the nonnegative flow value on the arc a for box i . The optimization problem can

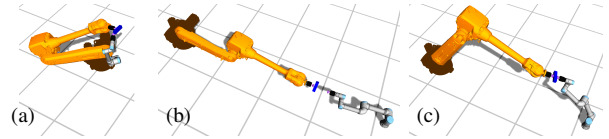


Fig. 2: Non-reachable robot pairs due to collisions (a) and kinematic limits (b), and a reachable robot pair (c)

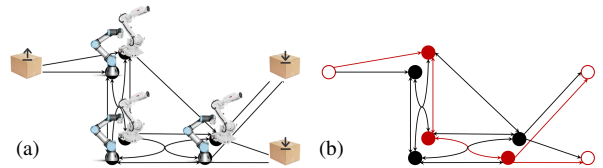


Fig. 3: The ground set and the corresponding graph (a) of the layout, where each grid point is assigned with two potential robots, and a feasible subgraph (b, red) extracted from it. We use hollow vertices to denote input/output locations and solid vertices to denote robots.

be formulated as:

$$\min_{\substack{s_a \in \{0,1\}, f_{a,i} \in \mathbb{R}_{\geq 0}, \\ a \in A, i \in \{1,2,\dots,N\}}} \sum_{a \in A_{\text{aux}}} w_a s_a, \quad (3a)$$

$$s.t. \quad \sum_{\substack{a \in A_{\text{aux}}, \\ \text{COOR}(a)=p}} s_a \leq 1, \quad \forall p \in P \quad (3b)$$

$$\forall i \in \{1,2,\dots,N\}, \quad f_{a,i} \leq s_a, \quad \forall a \in A \quad (3c)$$

$$\begin{aligned} \sum_{a \in \delta^+(v)} f_{a,i} - \sum_{a \in \delta^-(v)} f_{a,i} &= -1, \quad \forall v \in V_{\text{in}}, \\ \sum_{a \in \delta^+(v)} f_{a,i} - \sum_{a \in \delta^-(v)} f_{a,i} &= 1, \quad v = V_{\text{out},i}, \\ \sum_{a \in \delta^+(v)} f_{a,i} - \sum_{a \in \delta^-(v)} f_{a,i} &= 0, \quad \text{otherwise} \end{aligned} \quad (3d)$$

where $\text{COOR}(a)$ maps an auxiliary arc a to the location p of the corresponding robot, $\delta^+(v)/\delta^-(v)$ represents the inbound/outbound arc set of vertex v . Equation 3b avoid multiple robots being installed at the same location in space. Equation 3c restricts the flow value on all arcs not exceeding the capacity limits controlled by the selection variable. Equation 3d guarantees that the influx equals the outflux on all vertices for all flows, which ensures the existence of a flow that connects the input and output locations of each box.

Such a flow problem can be solved with any off-the-shelf MILP solver. When the solver converges, the solution is guaranteed to be optimal, upon which we can trace the optimal subgraph and generate the layout.

B. Task Scheduling

With an optimal subgraph of G computed, the robot assignment $(r_1^i, r_2^i, \dots, r_{N_i}^i)$ for delivery box i can be determined by tracing the shortest path connecting the box's input and output locations. Assuming that every robot takes equal time ΔT to transport a box, the task schedule for box i is $s^i([(k-1) \times \Delta T, k \times \Delta T]) = r_k^i, k \in \{1, \dots, N_i\}$.

We can further stack and shift single-box schedules to enable asynchronous delivery so that more than one box is handled at a time. Assuming that we are given a delivery order, we can make all delivery tasks start at the same time, and resolve conflicts, i.e., two boxes are delivered by the same robot at the same time, sequentially by delaying the delivery of the box later in the sequence slightly. To achieve shorter execution times for illustration purposes, we use a delivery order that prioritizes the longer graph transport path in the following sections and the supplementary video.

C. Motion Planning

With the task schedule specified, we refine the constraints stated in Eq. 1b to Eq. 1d into a trajectory optimization formulation. We discretize the trajectory into n time steps and let $\mathbf{x}_{r,t}$ be the joint values of robot r at time step t .

The joint angles are subjected to box constraints of the form $x_r^{\min} \leq \mathbf{x}_{r,t} \leq x_r^{\max}$ that correspond to the physical joint limit of the robot. We use $\mathbf{f}_r : \mathbb{R}^{d_i} \mapsto SE(3)$ for denoting the forward kinematic function that maps the joint state \mathbf{x}_r of robot r to an end effector pose in the world coordinate frame. Let Φ^i and Ψ^i be box i 's initial and goal pose in the world coordinate frame corresponding to its input and output locations.

1) *Kinematic switch constraints*: The pose of a box is constrained by the kinematic equations that are induced by the robot holding it. When the scheduling function s^i has a discontinuity, this set of constraints changes, and these moments are known as the kinematic switches. Every time a robot arm r picks up box i at time step t , its end effector's pose should match the box's initial pose Φ^i :

$$C_{\text{pick}} := \|\mathbf{f}_r(\mathbf{x}_{r,t}) - \Phi^i\| = 0 \quad (4)$$

Similarly, every time a robot arm places down a box:

$$C_{\text{place}} := \|\mathbf{f}_r(\mathbf{x}_{r,t}) - \Psi^i\| = 0 \quad (5)$$

We introduce a function $\text{REVERSE} : SE(3) \mapsto SE(3)$ to reverse an end effector's axes for handover with another end effector. Then, the constraint for handover:

$$C_{\text{hand}} := \|\mathbf{f}_{r_1}(\mathbf{x}_{r_1,t}) - \text{REVERSE}[\mathbf{f}_{r_2}(\mathbf{x}_{r_2,t})]\| = 0 \quad (6)$$

Given a task schedule, we define three sets PICK, PLACE, HAND to record all picking/placing/handover events.

2) *Collision avoidance constraints*: We attach a series of spheres to the links of robot arms to approximate their collision meshes. Collision-free trajectories are ensured by imposing a collision avoidance constraint of the form:

$$C_{\text{collision}} := \text{DIST}(\mathcal{K}_a(\mathbf{x}), \mathcal{K}_b(\mathbf{x})) > 0, \quad \forall a, b \in \mathcal{C} \quad (7)$$

where \mathcal{K}_a and \mathcal{K}_b denote a pair of forward kinematic functions for collision spheres $a, b \in \mathcal{C}$ in the scene and DIST computes the squared distance between spheres.

3) *Trajectory optimization*: By stacking all robot trajectories into \mathbf{x} , we can now write the trajectory optimization problem as:

$$\min_{\mathbf{x}} \quad \mathcal{O}(\mathbf{x}) \quad (8a)$$

$$s.t. \quad C_{\text{pick}} = 0, \quad \forall (i, r, \Phi^i, t) \in \text{PICK} \quad (8b)$$

$$C_{\text{place}} = 0, \quad \forall (i, r, \Psi^i, t) \in \text{PLACE} \quad (8c)$$

$$C_{\text{hand}} = 0, \quad \forall (r_1, r_2, t) \in \text{HAND} \quad (8d)$$

$$C_{\text{collision}} > 0, \quad \forall a, b \in \text{COLLISION} \quad (8e)$$

$$\mathbf{x}_r^{\min} \leq \mathbf{x}_{r,t} \leq \mathbf{x}_r^{\max}, \quad \forall r \in \mathcal{R} \quad (8f)$$

where $\mathcal{O}(\mathbf{x})$ is the objective function that penalizes joint velocities and accelerations of each robot:

$$\mathcal{O}(\mathbf{x}) = \sum_{r \in \mathcal{R}} \left[\beta_v \sum \|\dot{\mathbf{x}}_r\| + \beta_a \sum \|\ddot{\mathbf{x}}_r\| \right] \quad (9)$$

where $\beta_v, \beta_a \in \mathbb{R}$ are constant weights.

To solve the constrained non-convex optimization problem 8 numerically, we convert it to an unconstrained problem by applying quadratic and cubic penalty functions to the equality and inequality constraints respectively, and solve it using the Gauss-Newton method.

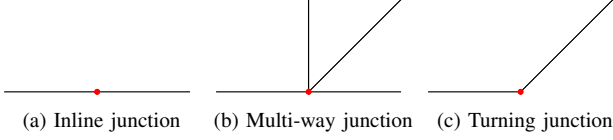


Fig. 4: Three types of junctions to connect belt segments

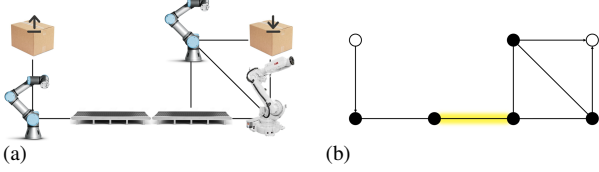


Fig. 5: A feasible layout with conveyor belts (a) and its corresponding graph representation (b), where the arc representing the inline junction is highlighted.

D. Modeling Conveyor Belts

We use a modular conveyor belt system consisting of unit segments of different orientations, which can be mounted on the floor grid points. For simplicity, we only allow four orientations: 0° , 45° , 90° , and 135° . Similar to the turntables in a real railway system, junctions are needed to connect conveyor belt segments and to direct boxes to different angles. We use three types of junctions as shown in Fig. 4: *inline junctions* are fictitious links that merge two conveyor belt segments into a longer, straight one; *turning junctions* redirect objects in a pair of pre-defined input/output directions; *multi-way junctions* redirect objects to multiple directions. Fig. 5 shows an exemplary feasible layout with conveyor belts. The arc representing an inline junction is highlighted.

a) Modeling conveyor belts and junctions in layout optimization: When constructing the reachability graph for the layout optimization, conveyor belt segments are treated similarly to robot arms. However, junctions require special treatment because their selection depends on the selected segments in their neighborhood. Below, we describe how each junction type is represented in the reachability graph, and the corresponding constraints to be added to the MILP formulation in Eq. 3.

An inline junction can only connect two adjacent belt segments that share the same orientation. Thus, for each pair of parallel segments at a grid point, we assign a new arc a^* connecting two adjacent belt segments r^+ , r^- , as shown in Fig. 6a. We record the set of inline junction's arcs as A_{inline} , and add the following constraints to Eq. 3:

$$s_{a^*} \leq s_{r^+}, \quad s_{a^*} \leq s_{r^-}, \quad \forall a^* \in A_{\text{inline}} \quad (10a)$$

$$\sum_{a^* \in \delta^+(r)} s_{a^*} \leq 1, \quad \sum_{a^* \in \delta^-(r)} s_{a^*} \leq 1, \quad \forall r \in \mathcal{R}_{\text{belt}} \quad (10b)$$

where Eq. 10a ensures an inline junction only appears when its parent and child segments are selected. Equation 10b ensure that each segment has at most one inline junction

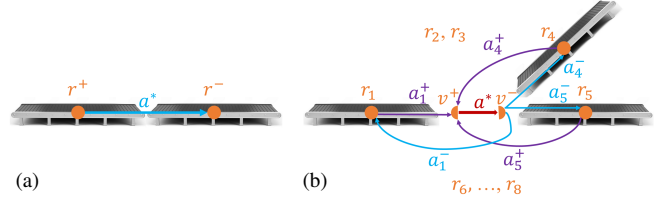


Fig. 6: Inline junctions (a) and multi-way/turning junctions (b) in the graph

starting from it and at most one ending at it so that the segments connected by an inline junction move in the same direction.

A multi-way junction can redirect among any subset of the eight segments that meet at a grid point. We represent it with a pair of vertices v^+ , v^- and an auxiliary arc a^* . In addition, we create eight new arcs a_i^+ connecting the neighboring segments to v^+ and eight new arcs a_i^- point out from v^- , as shown in Fig. 6b. Such graph construction will ensure that the junction arc a^* is selected when a flow exists between any pair among the eight segments.

A turning junction can be seen as a special case of a multi-way junction, where only two segments are connected. We can encode this with the following constraints:

$$\sum_{i=1}^8 s_{a_i^+} = 1, \quad \sum_{i=1}^8 s_{a_i^-} = 1, \quad (11)$$

Finally, we assign cost terms w_a for all the auxiliary arcs representing the conveyor belt segments and junctions. A unit-length conveyor belt segment requires a motor to operate its belt, so its cost is the sum of the belt cost and the motor cost. When multiple segments are connected by an inline junction, they share one motor, so their cost is the sum of the unit-length belt cost times the total length plus the cost of a motor. Inline junctions can reduce the motor cost of a composed conveyor belt system. Thus, their costs are set to negative to encourage their adoption. Multi-way and turning junctions have positive costs, with the multi-way junctions being more expensive due to their mechanical complexity.

b) Modeling conveyor belts in motion planning: We model a conveyor belt segment as a manipulator with multiple fictitious end effectors fixed to a prismatic joint. Each end effector of the conveyor belt can hold one box on the belt. The state vector of a belt r includes the prismatic joint's value $x_{r,t}^p$ and the grasp variables $x_{r,i}$ that describe the relative transformation between the end effector holding box i and the prismatic joint. Since the boxes cannot slide once placed on the belt, the grasp variables are time-independent and are shared across all time steps t . We assume that the conveyor belt maintains a constant speed, so $x_{r,t}^p$ is affine to the time step.

During the time steps when a belt is handling a box, we add the following constraints to the trajectory optimization Eq. 8 to ensure that the end effector holding the box i stays

Table I. Standard cost settings for experiments, normalized proportional to the market price.

UR5e	IRB4600	Belt (per meter)	Motor	Multi-way Junction	Turning Junction
1.0	3.0	0.2	0.1	0.1	0.05

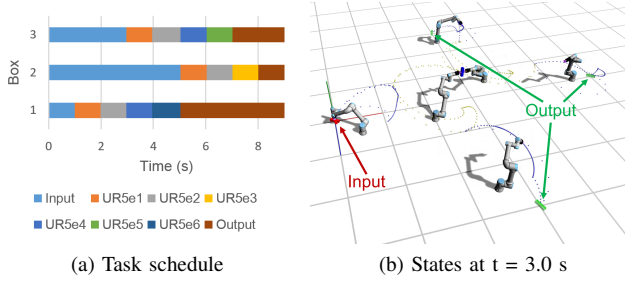


Fig. 7: Generated layout and task schedule with only UR5es

on the belt, not floating in the space along its extended line:

$$-\frac{1}{2}L_r < \mathbf{f}_{r,i}(x_{r,t}^p, x_{r,i}) \cdot x < \frac{1}{2}L_r, \forall t, s.t. s^i(t) = r \quad (12)$$

where t is the time step that the box i should stay on the belt, $\mathbf{f}_{r,i}$ is the forward kinematics function of end effector i in the base frame of the conveyor belt, and L_r is the belt length.

V. RESULTS

We evaluate the proposed layout design and planning framework on multiple simulated scenarios. The experiments were implemented in C++ and executed on a desktop computer with an Intel i7-8700K CPU @ 3.7 GHz and 32 GB RAM. We use Gurobi [19] as the MILP solver for layout optimization (Eq. 3). In all scenarios, the spacing between grid points for layout optimization is 0.5 m. The reference grids visualized in all the figures have a 1-meter spacing. The standard cost settings and running times for experiments are listed in Table I and Table II, respectively.

A. Delivery with only robot arms

We first demonstrate our algorithm on a scenario that has one input and three output locations, with only the UR5e arm available in \mathcal{R} . The computed optimal layout is shown in Fig. 7. Notable is that the solution places two robots diagonally in the center to split the delivery flow. Fig. 7a shows the task schedule generated using the task scheduling technique described in Section IV-B, where multiple boxes are handled simultaneously. Fig. 7b shows a moment when two robot arms hand over a box. The detailed motion can be found in the supplementary video material.

B. Impact of junction costs

In this experiment, we include conveyor belts and UR5e arm in the available robot set, and showcase how the layout optimization responds to different junction cost configurations. We normalize the price of a UR5e robot arm to 1.0

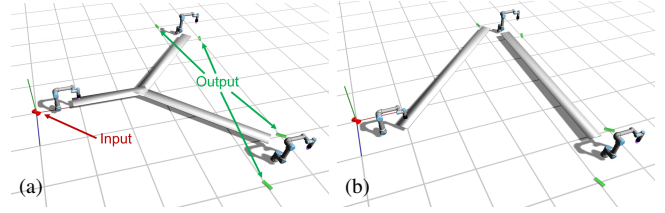


Fig. 8: Optimal layout for (a) lower and (b) higher junction costs.

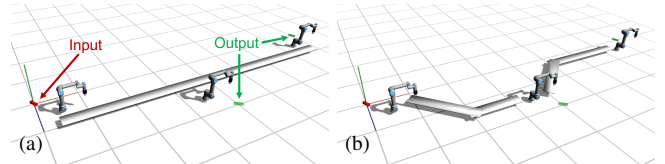


Fig. 9: Optimal layout for (a) higher and (b) lower motor costs.

and set the price of conveyor belts and junctions according to Table I. In Fig. 8a, we show the optimal layout that automatically groups the four outputs into two pairs, and assign each pair with a robot arm to unload. In the center, it chooses a multi-way junction to split the flow to different unloading robot arms. In contrast, after quadrupling the price of multi-way and turning junctions, the optimal layout in Fig. 8b uses two long belts with inline junctions instead of the more expensive multi-way junction.

C. Impact of motor cost

We showcase how the optimal layout changes the conveyor belt composition based on different motor cost configurations. For the standard cost settings, a long belt is chosen to carry all boxes, with one robot assigned at the side of the belt to unload the box (Fig. 9a). In contrast, in Fig. 9b, we reduce the motor cost to 0.02, and the algorithm then substitutes the long conveyor belt with several shorter ones, each with a separate motor, to reduce the total length.

D. Handling payload constraints

Our layout optimization can be configured to respond to payload constraints. In this experiment, we include boxes of two weights and introduce a new type of robot arm—IRB4600, which has a larger reach, larger payload limit, and higher cost. While the IRB4600 robot and the conveyor belt can handle both box weights, the UR5e robot can only handle the light box. This payload constraint can be enforced by setting $f_{a,i} = 0$ in Eq. 3, for a corresponding to the robot with a payload limit lower than the weight of box i . Under the same input and output locations, Fig. 10 shows the generated layouts corresponding to the same output locations, but different box weight distributions.

From Fig. 10, we can notice IRB4600s are positioned closer to heavy boxes since each heavy box requires an IRB4600 to carry and place down. In contrast, each light

Table II. MILP parameters and running time of each experiment.

Experiment	MILP parameters			Running Time (in seconds)		
	Number of variables		Number of constraints	Layout Optimization	Task Scheduling	Motion Planning
	Continuous	Binary				
Delivery with only robot arms	28995	9665	30554	0.38	0.001	1.36
Impact of junction costs (Cheap junctions)	95032	23758	112162	86.07	0.001	62.79
Impact of junction costs (Expensive junctions)	95032	23758	112162	10.33	0.001	45.32
Impact of motor cost (Expensive motors)	30724	15362	38654	10.73	0.001	5.09
Impact of motor cost (Cheap motors)	30724	15362	38654	7.91	0.001	24.88
Handling payload constraints (2 heavy & 1 light)	974832	324944	1005896	30.84	0.001	2.28
Handling payload constraints (1 heavy & 2 light)	974832	324944	1005539	32.31	0.001	5.23

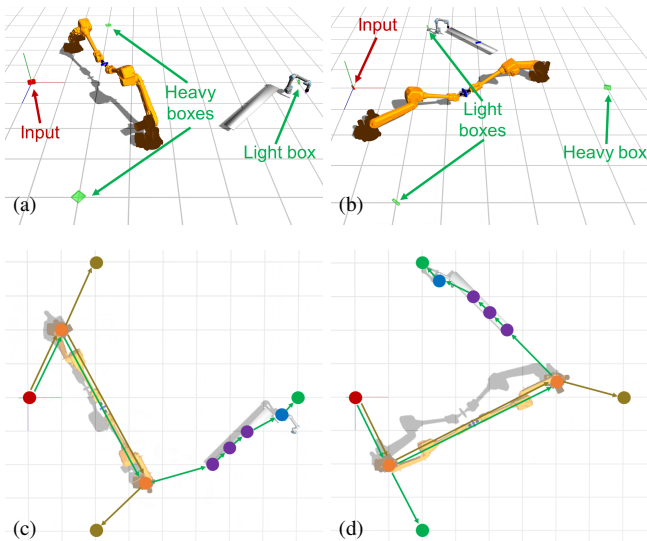


Fig. 10: Optimal Layout (a,b) and box delivery paths (c,d) when handling a scenario with two heavy boxes and one light box (a,c) and a scenario with one heavy box and two light boxes (b,d). Three types of robots — UR5e (blue), IRB4600 (orange), and conveyor belts (purple) — are employed.

box can be handled with a combination of UR5es and conveyor belts to save budget. Also, conveyor belts appear less frequently than in previous experiments since the large reachable area of the IRB4600 reduces the reliance on conveyor belts.

E. Comparison with A* search

Our graph-based layout optimization determines all robot placement *jointly* with connectivity enforced by flow constraints. An intuitive alternative way to solve this is to assign robots *procedurally* using a grid search to reach multiple destinations. We choose the A* algorithm as a baseline and compare it with our method on the test scenes in Fig. 11a. There are two output locations set symmetrically to the input. By adjusting the length and the width, we can change the grid size and, thus, the input size. The larger the length or width, the more grid points and corresponding robot candidates are considered in the optimization process. For simplicity, we

Table III. Running time of our algorithm and A* for layout optimization (in seconds)

Method	Length (m)			
	4	6	8	16
Ours	0.18	0.22	0.31	0.79
A*	0.62	22.51	(>86)	(>93)

only consider UR5e here and fix the width to 4 meters.

The input to the A* search is the position of all input/output locations, and the output is a robot placement to deliver all boxes with the goal of minimizing the total number of UR5e assigned. The state of the search is a set of grid position-robot pairs: $q = \{(p, r) \in P \times \mathcal{R}\}$. The neighbors of a given state q include all robot types assigned on reachable grid points, which makes the branching factor quite large. For the objective function $f(q) = g(q) + h(q)$, the current cost $g(q)$ considers the number of UR5e already selected in the path. The main challenge for making A* efficient is the design of an admissible, yet tight heuristic function, which is highly non-trivial in our multi-destination scenario with a large branching factor. We use an admissible heuristic function that computes the minimum number of UR5es needed to connect the farthest output location to the current reachable blob: $h(q) = \lceil \frac{1}{2l} \max_{i \in \{1, \dots, N\}} \min_{p \in q} \text{DIST}_i(p) \rceil$, where l denotes the maximal reach distance of UR5e and $\text{DIST}_i(p)$ denotes the distance from the grid point $p \in P$ to the output location of box i .

The running time of both methods for layout optimization is shown in Table III. For smaller input sizes, our method is significantly faster than A*. Once the length equals or exceeds 8 meters, A* fails to form a solution before running out of memory. Therefore, our graph-based layout optimization algorithm outperforms A* in running time and memory usage.

F. Scalability analysis for layout optimization

This section aims to provide a more detailed analysis of how our layout optimization scales with input size. Our goal is to allocate UR5e and conveyor belts to solve the same tasks shown in Fig. 11a, with varying length and width. Fig. 11b shows the optimal layouts, where orange dots stand for UR5e and purple segments stand for conveyor belts. An interesting

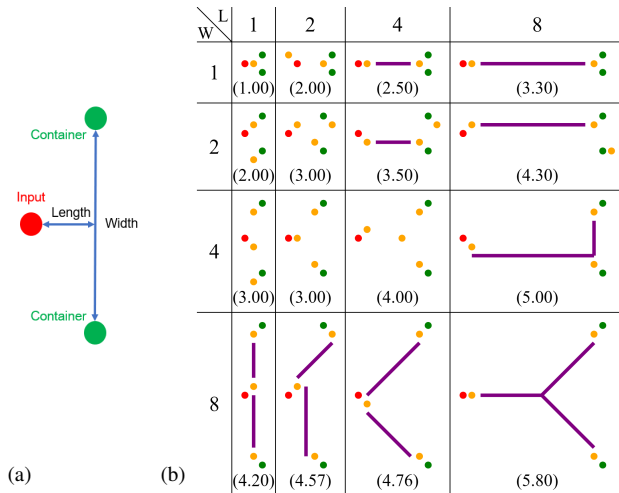


Fig. 11: Test scenes (a) from the scalability analysis and results (b) under different lengths and widths, showing optimal layouts and corresponding costs (in parentheses)

Table IV. Running time for layout optimization with different input sizes (in seconds)

Width (m) \ Length (m)	1	2	4	8
1	0.07	0.11	0.27	0.66
2	0.09	0.14	0.76	1.16
4	0.17	0.29	8.13	23.96
8	0.94	10.61	14.67	626.78

case is the $4m \times 4m$ one, where no conveyor belts appear, unlike other 4-meter-length cases. The algorithm decides that one robot arm is more cost-efficient than multiple short belts connected with a junction.

The running time of all scenes is shown in Table IV. We can tell the running time grows exponentially concerning the input size; the reason will be discussed in Section VI. Although the algorithm becomes inefficient with large-scale input, it remains acceptable for handling inputs of a reasonable size.

VI. DISCUSSION AND CONCLUSION

We have presented a novel flow-based method for layout optimization of multi-robot workspace, enabling finding the minimum-cost layout to achieve a series of delivery tasks. Our method additionally models conveyor belts as manipulators with multiple end effectors, integrating them alongside other robot arms in workspace design and motion planning. Finally, we have conducted experiments in simulations to reveal the computational and demonstrate the effectiveness of our method in complex scenarios.

Although our method performs better than A*, it still has difficulty scaling with the grid size due to the combinatorial nature of the layout optimization problem. A classic NP-complete problem, the Minimum Steiner Tree in graphs [20], can be solved by our formulation, thus making our optimization problem NP-hard and the runtime non-polynomial.

In our problem settings Eq. 1, we consider only robots mounted on the floor. Extending the candidate robots to include those in 3D spaces, such as ceil- or wall-mounted robot arms, would be an interesting direction for future work, as it could expand the reachable regions of robotic arms. Furthermore, we only require the delivery of each object to its output locations separately without considering the system’s throughput. Maximizing the system’s throughput within a limited budget is another area to explore.

REFERENCES

- [1] F. Zacharias, C. Borst, and G. Hirzinger, “Capturing robot workspace structure: representing robot capabilities,” in *2007 IEEE/RSJ International Conference on Intelligent Robots and Systems*, 2007, pp. 3229–3236.
- [2] A. Makhmal and A. K. Goins, “Reuleaux: Robot base placement by reachability analysis,” in *2018 Second IEEE International Conference on Robotic Computing (IRC)*, 2018, pp. 137–142.
- [3] M. Xu, J. Di, N. Das, and M. C. Yip, “Optimal multi-manipulator arm placement for maximal dexterity during robotics surgery,” in *2021 IEEE International Conference on Robotics and Automation (ICRA)*, 2021, pp. 9752–9758.
- [4] S. Ha, S. Coros, A. Alspach, J. Kim, and K. Yamane, “Computational co-optimization of design parameters and motion trajectories for robotic systems,” *The International Journal of Robotics Research*, vol. 37, no. 13-14, pp. 1521–1536, 2018.
- [5] J. Whitman and H. Choset, “Task-specific manipulator design and trajectory synthesis,” *IEEE Robotics and Automation Letters*, vol. 4, no. 2, pp. 301–308, 2018.
- [6] M. Toussaint, J.-S. Ha, and O. S. Oguz, “Co-optimizing robot, environment, and tool design via joint manipulation planning,” in *2021 IEEE International Conference on Robotics and Automation (ICRA)*, 2021, pp. 6600–6606.
- [7] S. Huber, R. Poranne, and S. Coros, “Designing actuation systems for animatronic figures via globally optimal discrete search,” *ACM Trans. Graph.*, vol. 40, no. 4, jul 2021. [Online]. Available: <https://doi.org/10.1145/3450626.3459867>
- [8] C. R. Garrett, R. Chitnis, R. Holladay, B. Kim, T. Silver, L. P. Kaelbling, and T. Lozano-Pérez, “Integrated task and motion planning,” *Annual review of control, robotics, and autonomous systems*, vol. 4, no. 1, pp. 265–293, 2021.
- [9] C. R. Garrett, T. Lozano-Pérez, and L. P. Kaelbling, “Pddlstream: Integrating symbolic planners and blackbox samplers via optimistic adaptive planning,” in *Proceedings of the international conference on automated planning and scheduling*, vol. 30, 2020, pp. 440–448.
- [10] M. Toussaint, “Logic-geometric programming: An optimization-based approach to combined task and motion planning,” in *IJCAI*, 2015, pp. 1930–1936.
- [11] T. Siméon, J.-P. Laumond, J. Cortés, and A. Sahbani, “Manipulation planning with probabilistic roadmaps,” *The International Journal of Robotics Research*, vol. 23, no. 7-8, pp. 729–746, 2004.
- [12] V. N. Hartmann, A. Orthey, D. Driess, O. S. Oguz, and M. Toussaint, “Long-horizon multi-robot rearrangement planning for construction assembly,” *IEEE Transactions on Robotics*, vol. 39, no. 1, pp. 239–252, 2022.
- [13] J. Envall, R. Poranne, and S. Coros, “Differentiable task assignment and motion planning,” in *2023 IEEE/RSJ International Conference on Intelligent Robots and Systems (IROS)*. IEEE, 2023, pp. 2049–2056.
- [14] R. Shome and K. E. Bekris, “Anytime multi-arm task and motion planning for pick-and-place of individual objects via handoffs,” in *2019 International Symposium on Multi-Robot and Multi-Agent Systems (MRS)*. IEEE, 2019, pp. 37–43.
- [15] Y. Zhang, M. C. Fontaine, V. Bhatt, S. Nikolaidis, and J. Li, “Multi-robot coordination and layout design for automated warehousing,” in *Proceedings of the International Joint Conference on Artificial Intelligence (IJCAI)*, 2023, pp. 5503–5511.
- [16] Y. Zhang, M. Fontaine, V. Bhatt, S. Nikolaidis, and J. Li, “Arbitrarily scalable environment generators via neural cellular automata,” *Advances in Neural Information Processing Systems*, vol. 36, 2024.
- [17] Z. Gao and A. Prorok, “Environment optimization for multi-agent navigation,” in *2023 IEEE International Conference on Robotics and Automation (ICRA)*. IEEE, 2023, pp. 3440–3446.

- [18] Z. Gao and A. Prorok, "Constrained environment optimization for prioritized multi-agent navigation," *IEEE Open Journal of Control Systems*, 2023.
- [19] Gurobi Optimization, LLC, "Gurobi Optimizer Reference Manual," 2024. [Online]. Available: <https://www.gurobi.com>
- [20] R. M. Karp, *Reducibility among combinatorial problems*. Springer, 2010.